Journal of Magnetic Resonance 195 (2008) 23–32

Contents lists available at ScienceDirect

Journal of Magnetic Resonance

journal homepage: www.elsevier.com/locate/jmr

A tensor approach to double wave vector diffusion-weighting experiments on restricted diffusion

Jürgen Finsterbusch *, Martin A. Koch

Department of Systems Neuroscience, University Medical Center Hamburg–Eppendorf, 20246 Hamburg, Germany
Neuroimage Nord, University Medical Centers Hamburg–Kiel–Lübeck, Germany

ARTICLE INFO

Article history:
Received 27 June 2008
Revised 4 August 2008
Available online 14 August 2008

Keywords:
Double wave vector diffusion weighting
Tensor
Restricted diffusion
Cell size
Pore size

ABSTRACT

Previously, it has been shown theoretically that in case of restricted diffusion, e.g. within isolated pores or cells, a measure of the pore size, the mean radius of gyration, can be estimated from double wave vector diffusion-weighting experiments. However, these results are based on the assumption of an isotropic orientation distribution of the pores or cells which hampers the applicability to samples with anisotropic or unknown orientation distributions, such as biological tissue. Here, the theoretical considerations are re-investigated and generalized in order to describe the signal dependency for arbitrary orientation distributions. The second-order Taylor expansion of the signal delivers a symmetric rank-2 tensor with six independent elements if the two wave vectors are concatenated to a single six-element vector. With this tensor approach the signal behavior for arbitrary wave vectors and orientation distributions can be described as is demonstrated by numerical simulations. The rotationally invariant trace of the tensor represents a pore size measure and can be determined from three orthogonal directions with parallel and antiparallel orientation of the two wave vectors. Thus, the presented tensor approach may help to improve the applicability of double wave vector diffusion-weighting experiments to determine pore or cell sizes, in particular in biological tissue.

© 2008 Elsevier Inc. All rights reserved.

1. Introduction

Extensions of the pulsed-gradient diffusion-weighted experiment [1] involving two diffusion-weighting periods applied successively in a single experiment, have been first presented by Cory et al. [2] and Callaghan et al. [3]. Whereas the pulse sequences used by Cory et al. aimed at assessing the leakage and eccentricity of diffusion in pores [2], Callaghan et al. investigated the temporal correlation of displacements in the two successive diffusion-weighting intervals [3]. Because in the limit of short gradient pulses the diffusion weighting can be described by a wave vector when following the analogy to scattering experiments [4], these approaches can be considered as the two or double wave vector extensions of the standard, single wave vector experiment.

Later, Mitra theoretically investigated the properties of double wave vector experiments in more detail [5]. He considered diffusion in isolated pores that is assumed to be fully restricted on the time scale of the diffusion times and derived general expressions for the signal behavior depending on the two wave vectors for an infinitely short and an infinitely long mixing time between the two diffusion weightings.

From the expression for an infinite mixing time, he concluded that samples with spherical and ellipsoidal pores can be distinguished when comparing double wave vector experiments with parallel and orthogonal wave vectors even if an isotropic orientation distribution of the pores is present in the sample. This is of particular interest as both such samples macroscopically appear isotropic and cannot be distinguished in a standard, single wave vector diffusion-weighting experiment. Thus, double wave vector diffusion weighting could be used to detect and measure anisotropy on a microscopic scale.

This finding has been analyzed for ellipsoidal pores in more detail by Cheng et al. [6] who derived expressions for the signal behavior depending on the ellipsoid's axes, and confirmed them with numerical simulations and experimentally on yeast cells. More recently, the effect was used to demonstrate microscopic anisotropy within gray matter of monkey brain *in vitro* and pig spinal cord *ex vivo* [7–9]. Callaghan et al. [10] presented a full 2D extension of the experiment including an analysis using the inverse Laplace transformation which in samples with microscopic anisotropy yields typical off-diagonal patterns in the 2D spectrum of the diffusion coefficient as was demonstrated for liquid crystals.

For the other case, i.e. for a vanishing mixing time, Mitra found for an isotropic orientation distribution that the signal shows a cosine dependency on the relative angle between the two wave

* Corresponding author. Fax: +49 40 42803 9955.
E-mail address: j.finsterbusch@uke.uni-hamburg.de (J. Finsterbusch).

1090-7807/$ - see front matter © 2008 Elsevier Inc. All rights reserved.
doi:10.1016/j.jmr.2008.08.003

vectors $\mathbf{q_i}$ in the second order of the q expansion, with the modulation amplitude increasing with pore size. Thus, pore or compartment sizes can be estimated under these conditions, e.g. by considering the signal difference of two measurements with parallel and antiparallel wave vector orientations, respectively. Experimental demonstrations of this effect have been presented recently in biological samples [11,12] and extracted pig spinal cord [13].

Although the experimental results are very promising, in particular for biomedical research, the assumptions underlying the theoretical derivation, either spherical pores or cells or an isotropic orientation distribution, are commonly not fulfilled in biological tissue. Moreover, a re-calculation for a given pore shape or orientation distribution is of limited value because these properties are usually unknown or cannot be taken for granted in the sample under investigation. Thus, the results presented by Mitra may be considered unsatisfying for a reliable and accurate cell size estimation in practice.

As a possible solution to this problem, quasi-isotropic acquisition schemes could be used. Thereby, the parallel–antiparallel effect would be measured for a large number of isotropically distributed directions of the diffusion weighting. Averaging the macroscopic signals of these acquisitions is equivalent to averaging microscopic signals of pores with different orientations to the macroscopic signal obtained in samples with isotropic orientation distribution. However, a large number of directions is required to ensure a sufficient sampling of the directions, resulting in a correspondingly long acquisition time.

In the present study, the theoretical approach used by Mitra is re-investigated with the aim to derive an orientation-independent measure of the pore or cell size which can be used for arbitrary orientation distributions. The signal behavior of the double wave vector experiment with infinitely short fill time can be described by a rank-2 tensor in the second order of q which delivers the tensor's trace as a rotationally invariant, and thus orientation-independent, measure for the pore or cell size. The equivalence to the result presented by Mitra is shown and a "reduced" tensor formalism is introduced that considers parallel and antiparallel wave vector orientations only. Numerical simulations demonstrate the feasibility of the tensor approaches to describe the observed signal behavior and to estimate pore or cell sizes from experiments.

2. Theory

2.1. Isotropic orientation distribution

Mitra has evaluated the NMR signal M observed in a double wave vector diffusion-weighting experiment with wave vectors $\mathbf{q_1}$ and $\mathbf{q_2}$ in case of fully restricted diffusion in isolated pores [5]. In the short-pulse approximation ($\delta \to 0$) and under the assumptions that the time τ_D a spin typically requires to diffuse over a distance comparable to the compartment size is short compared to the diffusion time Δ ($\tau_D \ll \Delta$) and that the mixing time between the successive diffusion weightings, τ_m, is negligible ($\tau_m = 0$), he found

$$M(\mathbf{q_1},\mathbf{q_2}) \propto \sum_i \tilde{\rho}_i(\mathbf{q_1})\tilde{\rho}_i(\mathbf{q_2})\tilde{\rho}_i(-\mathbf{q_1}-\mathbf{q_2}) \tag{1}$$

with $\tilde{\rho}_i$ being the Fourier transformation of the spatial distribution of the spin density $\rho_i(\mathbf{r})$ within the ith pore,

$$\tilde{\rho}_i(\mathbf{q}) = \int_{\text{pore}} \rho_i(\mathbf{r}) e^{i\mathbf{qr}}\, d\mathbf{r}, \tag{2}$$

and the summation being performed over all pores of the sample. The first two factors describe the effect of the diffusion weighting of the individual wave vectors $\mathbf{q_i}$ while the third factor represents their interaction and yields the features unique to the double wave vector experiment.

For the case of $|\mathbf{q_1}| = |\mathbf{q_2}| = q$, $\rho(\mathbf{r}) = \rho$, and an isotropic orientation distribution of the pores, Mitra obtained for the Taylor expansion of Eq. (1) to second order

$$M(q,\theta) \propto 1 - \frac{1}{3}q^2\langle R^2\rangle(2+\cos\theta) + \mathcal{O}(q^3) \tag{3}$$

with

$$\langle R^2\rangle = \int_{\text{pore}} r^2\, d\mathbf{r}, \tag{4}$$

called the pore's mean radius of gyration, and the angle between the two wave vectors θ. Thus, the NMR signal exhibits a cosine-shaped angular dependency on θ, introduced by the interaction term, whose modulation amplitude reflects the effective pore size.

Two other properties inherent to Eq. (3) are interesting: (i) the diffusion-induced signal decay of wave vectors enclosing angles of 0°, 90°, and 180° exhibit ratios of 3:2:1 and (ii) $\langle R^2\rangle$ can also be determined by varying q for a fixed θ.

2.2. Arbitrary orientation distributions

To obtain a more general description of the signal behavior that (i) is applicable to arbitrary orientation distributions and (ii) offers an approach to determine a rotationally invariant measure of the effective pore size, the expansion of Eq. (1) will be re-investigated in the following paragraphs.

Initially, a single pore orientation is considered. The sum signal then is proportional to that of an individual pore, i.e.

$$M(\mathbf{q_1},\mathbf{q_2}) \propto \tilde{\rho}(\mathbf{q_1})\tilde{\rho}(\mathbf{q_2})\tilde{\rho}(-\mathbf{q_1}-\mathbf{q_2}), \tag{5}$$

where the pore index i has been dropped for the sake of clarity. Because in general $\mathbf{q_1}$ and $\mathbf{q_2}$ are independent variables, $M(\mathbf{q_1},\mathbf{q_2})$ can be considered as a function of the six-element vector $\mathbf{Q} = (\mathbf{q_1}^T, \mathbf{q_2}^T)^T$, i.e.

$$Q_i = \begin{cases} (\mathbf{q_1})_i & \text{for } i = 1,2,3 \\ (\mathbf{q_2})_{i-3} & \text{for } i = 4,5,6 \end{cases}. \tag{6}$$

Eq. (5) then can be re-written as

$$M(\mathbf{Q}) \propto \tilde{\rho}_1(\mathbf{Q})\tilde{\rho}_2(\mathbf{Q})\tilde{\rho}_3(\mathbf{Q}) \tag{7}$$

with the individual factors also being described as functions of $\mathbf{Q}$ as well:

$$\begin{aligned} \tilde{\rho}_1(\mathbf{Q}) &= \tilde{\rho}(Q_1,Q_2,Q_3) = \tilde{\rho}(\mathbf{q_1}), \\ \tilde{\rho}_2(\mathbf{Q}) &= \tilde{\rho}(Q_4,Q_5,Q_6) = \tilde{\rho}(\mathbf{q_2}), \\ \tilde{\rho}_3(\mathbf{Q}) &= \tilde{\rho}(-Q_1-Q_4,-Q_2-Q_5,-Q_3-Q_6) = \tilde{\rho}(-\mathbf{q_1}-\mathbf{q_2}). \end{aligned} \tag{8}$$

The Taylor expansion of a function of n variables x_i up to the second order,

$$\begin{aligned} f(x_1,\ldots,x_n) = f(0,\ldots,0) &+ \sum_i x_i \frac{\partial}{\partial x_i} f(x_1,\ldots,x_n)\Big|_{x_1=\cdots=x_n=0} \\ &+ \frac{1}{2}\sum_{i,j} x_i x_j \frac{\partial}{\partial x_i}\frac{\partial}{\partial x_j} f(x_1,\ldots,x_n)\Big|_{x_1=\cdots=x_n=0} + \cdots, \end{aligned} \tag{9}$$

can be written as

$$f(\mathbf{x}) = a + \mathbf{x}^T\mathbf{b} + \frac{1}{2}\mathbf{x}^T\underline{\underline{\mathbf{C}}}\mathbf{x} + \cdots \tag{10}$$

when using $\mathbf{x} = (x_i,\ldots,x_n)^T$, $a = f(0)$, the vector $\mathbf{b}$ with

$$b_i = \frac{\partial}{\partial x_i} f(\mathbf{x})\Big|_{\mathbf{x}=0}, \tag{11}$$

and the rank-2 tensor $\underline{\underline{\mathbf{C}}}$ with

$$C_{ij} = \frac{\partial}{\partial x_i}\frac{\partial}{\partial x_j} f(\mathbf{x})\bigg|_{\mathbf{x}=0}. \tag{12}$$

The expansion of Eq. (7) up to second order can be written as the product of the expansions of the individual factors $\tilde{\rho}_j$ up to the same order. Thus, a closer look to the expansion of Eq. (2) is helpful which delivers

$$\tilde{\rho}(\mathbf{q}) = V + \mathrm{i}\mathbf{q}^{\mathrm{T}} \int_{\mathrm{pore}} \rho(\mathbf{r})\mathbf{r}\,\mathrm{d}\mathbf{r} - \frac{1}{2}\mathbf{q}^{\mathrm{T}}\underline{\underline{\mathbf{R}}}\mathbf{q} + \mathcal{O}(q^3), \tag{13}$$

where V denotes the pore volume and the elements of the 3×3 tensor $\underline{\underline{\mathbf{R}}}$ are given by

$$R_{ij} = \int_{\mathrm{pore}} \rho(\mathbf{r}) r_i r_j \,\mathrm{d}\mathbf{r}. \tag{14}$$

The first order term vanishes if the pore's center of gravity is chosen as the origin of the coordinate system, i.e.

$$\tilde{\rho}(\mathbf{q}) = V - \frac{1}{2}\mathbf{q}^{\mathrm{T}}\underline{\underline{\mathbf{R}}}\mathbf{q} + \mathcal{O}(q^3). \tag{15}$$

Thus, the expansion of the individual $\tilde{\rho}_j(\mathbf{Q})$ yields

$$\begin{aligned}
\tilde{\rho}_1(\mathbf{Q}) &= V - \tfrac{1}{2}\mathbf{Q}^{\mathrm{T}}\begin{pmatrix} \underline{\underline{\mathbf{R}}} & 0 \\ 0 & 0 \end{pmatrix}\mathbf{Q} + \mathcal{O}(Q^3), \\
\tilde{\rho}_2(\mathbf{Q}) &= V - \tfrac{1}{2}\mathbf{Q}^{\mathrm{T}}\begin{pmatrix} 0 & 0 \\ 0 & \underline{\underline{\mathbf{R}}} \end{pmatrix}\mathbf{Q} + \mathcal{O}(Q^3), \\
\tilde{\rho}_3(\mathbf{Q}) &= V - \tfrac{1}{2}\mathbf{Q}^{\mathrm{T}}\begin{pmatrix} \underline{\underline{\mathbf{R}}} & \underline{\underline{\mathbf{R}}} \\ \underline{\underline{\mathbf{R}}} & \underline{\underline{\mathbf{R}}} \end{pmatrix}\mathbf{Q} + \mathcal{O}(Q^3).
\end{aligned} \tag{16}$$

The expansion of Eq. (7) to second order therefore does not contain products of derivatives of the individual terms but consists only of a constant term and the sum of the individual second order terms and is given by

$$M(\mathbf{Q}) \propto V - \frac{1}{2}\mathbf{Q}^{\mathrm{T}}\underline{\underline{\mathbf{T}}}\mathbf{Q} \tag{17}$$

with

$$\underline{\underline{\mathbf{T}}} = \begin{pmatrix} 2\underline{\underline{\mathbf{R}}} & \underline{\underline{\mathbf{R}}} \\ \underline{\underline{\mathbf{R}}} & 2\underline{\underline{\mathbf{R}}} \end{pmatrix}. \tag{18}$$

These equations have been derived under the assumption of a single pore population. For multiple pore populations, e.g. with different orientations, pore shapes or pore sizes, the contributions of the individual populations simply need to be summed up according to

$$\begin{aligned}
V &= \sum_i p_j V_j, \\
\underline{\underline{\mathbf{R}}} &= \sum_i p_j \underline{\underline{\mathbf{R}}}_j,
\end{aligned} \tag{19}$$

where j identifies the population and the p_j represent their volume fraction.

Thus, a generalized description of the expected signal behavior in a double wave vector experiment with $\tau_{\mathrm{m}} = 0$ is obtained for arbitrary $\mathbf{Q}$, i.e. wave vectors $\mathbf{q_1}$ and $\mathbf{q_2}$. The equivalence to the result reported by Mitra for the special case of an isotropic orientation distribution and $|\mathbf{q_1}| = |\mathbf{q_2}| = q$ is shown in Appendix A.

It should be noted that Eq. (17) in general does not imply a cosine-shaped modulation of the signal upon changing θ. This is due to the fact that for non-spherical pores or cells the signal attenuation of each wave vector's diffusion weighting depends on the orientation of the corresponding wave vector with respect to the pores which in general changes when varying θ. This modulation is superimposed to the restriction effect and can lead to a more complex angular modulation as will be demonstrated below.

2.3. Pore size measure

Because $R_{ij} = R_{ji}$, $\underline{\underline{\mathbf{T}}}$ is also symmetric and has only six independent elements that are sufficient to describe the experiment for arbitrary $\mathbf{Q}$, i.e. wave vectors $\mathbf{q_1}$ and $\mathbf{q_2}$. Similar to the well-known diffusion tensor, the T_{ij} can be determined from six measurements with non-collinear $\mathbf{Q_k}$ if the signal without diffusion weighting is known, e.g. from a separate acquisition.

A rotationally invariant measure of the effective pore size within the sample, R_{eff}, can be derived from the trace of $\underline{\underline{\mathbf{T}}}$ which is proportional to the trace of $\underline{\underline{\mathbf{R}}}$:

$$\begin{aligned}
R_{\mathrm{eff}}^2 &= \frac{1}{4}\mathrm{Tr}(\underline{\underline{\mathbf{T}}}) = \mathrm{Tr}(\underline{\underline{\mathbf{R}}}) = \sum_j R_{jj} = \sum_j \sum_i \int_{\mathrm{pore}_i} \rho_i(\mathbf{r}) r_j^2 \,\mathrm{d}\mathbf{r} \\
&= \sum_i \int_{\mathrm{pore}_i} \rho_i(\mathbf{r}) \sum_j r_j^2 \,\mathrm{d}\mathbf{r} = \sum_i \int_{\mathrm{pore}_i} \rho_i(\mathbf{r}) r^2 \,\mathrm{d}\mathbf{r},
\end{aligned} \tag{20}$$

or in case of $\rho_i(\mathbf{r}) = \rho$

$$R_{\mathrm{eff}}^2 = \mathrm{Tr}(\underline{\underline{\mathbf{R}}}) = \rho \sum_i \int_{\mathrm{pore}_i} r^2 \,\mathrm{d}\mathbf{r}. \tag{21}$$

R_{eff} can be determined from three acquisitions with appropriate $\mathbf{Q_k}$ if the signal without diffusion weighting is known. It does not depend on the pore orientation distribution and can also be applied to a mixture of pore populations. It then represents the square root of the weighted average of the $R_{\mathrm{eff}\,j}^2$ of the individual pore populations.

Interestingly, the theoretical framework to estimate pore sizes presented in the last paragraphs does not require the usage of two wave vectors, neither for the determination of R_{eff} nor to calculate all elements of $\underline{\underline{\mathbf{T}}}$. This is due to the fact that the elements reflecting the specific interaction effect of both wave vectors, the "off-diagonal" sub-matrices of $\underline{\underline{\mathbf{T}}}$ ($2\underline{\underline{\mathbf{R}}}$), are multiples of the elements describing the effects of the single wave vectors, the diagonal submatrices ($\underline{\underline{\mathbf{R}}}$). For instance, $\underline{\underline{\mathbf{R}}}$, and thereby $\underline{\underline{\mathbf{T}}}$, can also be determined by using a single wave vector ($\mathbf{q_2} = \mathbf{0}$) experiment with different orientations of $\mathbf{q_1}$ and a measurement without diffusion weighting. This is similar to the observation that $\langle R^2 \rangle$ of Eq. (3) can be determined from two acquisitions with different q without changing θ. However, it is shown in the next paragraphs that ambiguities present in single wave vector experiments, e.g. introduced by a compartment with unrestricted diffusion, can be resolved with the double wave vector experiment.

2.4. Contributions of Gaussian diffusion

Consider signal contributions from free diffusing spins, e.g. those that do not "see" the pore boundaries within the diffusion time used or are outside of any pore boundaries as in extracellular space in biological tissue. The signal decay of those spins in the double wave vector experiment is given by

$$M_{\mathrm{free}}(\mathbf{q_1}, \mathbf{q_2}) \propto \mathrm{e}^{-\Delta_{\mathrm{eff}} D q_1^2} \mathrm{e}^{-\Delta_{\mathrm{eff}} D q_2^2} = \mathrm{e}^{-\Delta_{\mathrm{eff}} D (q_1^2 + q_2^2)} \tag{22}$$

with the free diffusion coefficient D and the effective diffusion time $\Delta_{\mathrm{eff}} = \Delta - \delta/3$. Expanded to second order,

$$M_{\mathrm{free}}(\mathbf{q_1}, \mathbf{q_2}) \propto 1 - \Delta_{\mathrm{eff}} D (q_1^2 + q_2^2) + \mathcal{O}(q^3) \tag{23}$$

is obtained which in the tensor formalism and considered as a function of $\mathbf{Q}$ yields

$$M_{\mathrm{free}}(\mathbf{Q}) \propto 1 - \Delta_{\mathrm{eff}} D \mathbf{Q}^{\mathrm{T}} \begin{pmatrix} \underline{\underline{\mathbf{1}}} & 0 \\ 0 & \underline{\underline{\mathbf{1}}} \end{pmatrix} \mathbf{Q}. \tag{24}$$

Analogously, the signal of a compartment with anisotropic Gaussian diffusion which can be described by the well-known diffusion tensor $\underline{\underline{\mathbf{D}}}$, can be described by

$$M_{\underline{\underline{\mathbf{D}}}}(\mathbf{Q}) \propto 1 - \Delta_{\mathrm{eff}}\mathbf{Q}^{\mathrm{T}}\begin{pmatrix}\underline{\underline{\mathbf{D}}} & 0\\ 0 & \underline{\underline{\mathbf{D}}}\end{pmatrix}\mathbf{Q}. \quad (25)$$

In these cases, the diagonal sub-matrices that describe the single wave vector contributions, are distorted by the contributions of the compartment with Gaussian diffusion. This reflects the fact that the signal decay with q observed in a single wave vector experiment cannot be unambiguously assigned to diffusion in a hindered but unrestricted compartment or to a restricted compartment. Thus, an estimation of the pore or cell size with a single wave vector experiment is hampered in the presence of compartments with Gaussian diffusion. However, the off-diagonal sub-matrices that reflect the interaction of the two wave vectors, do not change. Thus, the double wave vector effect which is observed upon variation of θ is unaffected by signal contributions from free diffusion and represents a straightforward access to the restricted compartment.

2.5. Difference of parallel and antiparallel orientations

In practice, the easiest and most reliable approach to measure the restriction effect and estimate R_{eff} is to compare acquisitions with parallel and antiparallel orientations of the two wave vectors. This avoids signal modulations present in samples with non-spherical cells and non-isotropic orientation distributions and minimizes anisotropy effects due to hardware inadequacies like differing eddy-current behavior or gradient scaling mismatches between the different physical gradient axes. Furthermore, it is the most sensitive setup because it reveals the maximum signal difference of the underlying restriction effect.

Considering the signal difference of parallel and antiparallel wave vector orientations, some simplification of Eq. (17) can be achieved. Assuming $\mathbf{q} = \mathbf{q_1} = \pm\mathbf{q_2}$, the signal difference of $\mathbf{Q}_- = (\mathbf{q}^{\mathrm{T}}, -\mathbf{q}^{\mathrm{T}})^{\mathrm{T}}$ and $\mathbf{Q}_+ = (\mathbf{q}^{\mathrm{T}}, \mathbf{q}^{\mathrm{T}})^{\mathrm{T}}$ contains only the off-diagonal matrices of $\underline{\underline{\mathbf{T}}}$ and can be re-written as a function of $\mathbf{q}$ by

$$\Delta M(\mathbf{q}) = \frac{1}{2}\left(\mathbf{q}^{\mathrm{T}}\underline{\underline{\mathbf{R}}}\mathbf{q} + \mathbf{q}^{\mathrm{T}}\underline{\underline{\mathbf{R}}}\mathbf{q} - \mathbf{q}^{\mathrm{T}}\underline{\underline{\mathbf{R}}}(-\mathbf{q}) - (-\mathbf{q})^{\mathrm{T}}\underline{\underline{\mathbf{R}}}\mathbf{q}\right) = 2\mathbf{q}^{\mathrm{T}}\underline{\underline{\mathbf{R}}}\mathbf{q} = \mathbf{q}^{\mathrm{T}}2\underline{\underline{\mathbf{R}}}\mathbf{q}. \quad (26)$$

Thus, the signal difference observed in experiments with parallel and antiparallel wave vector orientations is fully described by the rank-2 tensor $\underline{\underline{\mathbf{R}}}$ with its six independent elements for any orientation of $\mathbf{q}$. It should be emphasized that this result is independent of Gaussian diffusion contributions, which represents the advantage of the double wave vector experiment. For an isotropic orientation distribution and $\rho(\mathbf{r}) = \rho$, Eq. (26) simplifies to the result of Mitra

$$\Delta M(\mathbf{q}) \propto \frac{2}{3}\rho q^2\langle R^2\rangle. \quad (27)$$

3. Experimental

To evaluate the presented tensor approach, a self-written IDL algorithm (version 6.4, ITT Visual Information Solutions, Boulder, USA) was used to simulate the MR signal of diffusing spins in double wave vector experiments and analyze it with respect to the signal behavior predicted by Eqs. (17) and (26). Spherical pores and prolate spheroidal pores (semi-principal axes ratio of 1.825) yielding identical $\langle R^2\rangle$ and with impermeable boundaries were considered in separate simulations. Relaxation effects were neglected.

Ten thousand spins were observed during the simulation with random starting points within the pore. For each time unit a random, Gaussian displacement was applied with a random step direction. Diffuse reflection was assumed at the pore boundaries: in case the new position of a particle calculated was outside of the pore, an additional calculation step was introduced starting at the intersection of the particle's trajectory with the pore boundary with a new random step direction and a step length corresponding to the remaining displacement. Thereby, repetitive reflections at the pore boundary within a single time step were allowed until the full desired displacement was realized.

For the pore and displacement parameters chosen, τ_{D} can be estimated to values of about 100 time units for the spherical and between 56 and 187 time units for the spheroidal pores, respectively. The gradient pulse duration δ and the mixing time τ_{m} were one time unit. This is the best approximation to the short-pulse assumption that avoids an angular dependency of the diffusion-weighting b value which occurs for $\tau_{\mathrm{m}} < \delta$. Δ was 3000 time units and thus well above τ_{D}.

A fixed orientation of the pores was used with the long axis of the spheroidal pores oriented along x. For all simulations $\mathbf{q_1} = \mathbf{q_2}$ was assumed. The different direction schemes used for the orientations of the two wave vectors in the individual simulations are shown in Fig. 1 and will be explained in more detail in the following paragraphs. As a simple approach for a double wave vector experiment to assess the modulation of the signal with the angle θ enclosed by the two wave vectors, wave vector orientations within a plane were simulated, e.g. as shown in Fig. 1a ("circle" scheme). Thereby, a fixed orientation was chosen for the first wave vector (x in Fig. 1a) while the second uniformly sampled 72 directions on a circle (in Fig. 1a in the xy plane) to cover the full angular range of θ. These simulations were performed with the xy, xz, and yz planes as the circle plane and the first wave vector oriented along x and y, x and z, and y and z, respectively, yielding six modulation curves.

For spherical pores, the angular dependency of the MR signal in these simulations would correspond to the cosine function in Eq. (3) and would be independent of the orientation of the first wave vector or the circle plane. For spheroidal pores, however, a more complex dependency is expected which depends on the chosen orientations of the circle plane and the first wave vector and which can be described by Eq. (17). Simulations with these circle direction schemes were performed (i) to demonstrate the variability of the angular signal modulation present in non-isotropic pore distributions and (ii) to confirm the agreement of the observed modulation with that described by Eq. (17) for a simple double wave vector experiment. The latter was achieved using a Levenberg–Marquardt algorithm to fit the simulated data to Eq. (17) for each of the six curves independently and to estimate the pore geometry parameters within the circle plane from the fit parameter.

The pore size determined with the circle scheme generally depends on the relative orientation of the circle with respect to the pores, which usually is unknown in most experiments. Thus, an extended direction scheme which uniformly covers a sphere can be used in experiments to yield an pore size estimate that is independent of the pore orientation distribution. This is due to the fact that the signal observed in an isotropic orientation distribution of the pores for two (fixed) wave vectors that span an angle θ is equivalent to that obtained for a fixed pore orientation and isotropically distributed wave vectors if the averaged signal of all wave vector combinations that enclose the same angle θ is taken. Or, in other words, the requirement of isotropy that is needed for a proper, orientation-independent pore estimate is "moved" from the pore orientation distribution in the sample to the wave vectors applied in the experiment.

For the "isotropic" direction scheme used in the corresponding simulations, both wave vectors were uniformly distributed over a sphere (Fig. 1b). Polar coordinates of the diffusion gradient directions for the first wave vector were determined analytically on 36 circles of latitude in steps of 5°. On each circle, equidistant directions were defined with the number of directions proportional to the circle's circumference and a maximum number of 72 on the

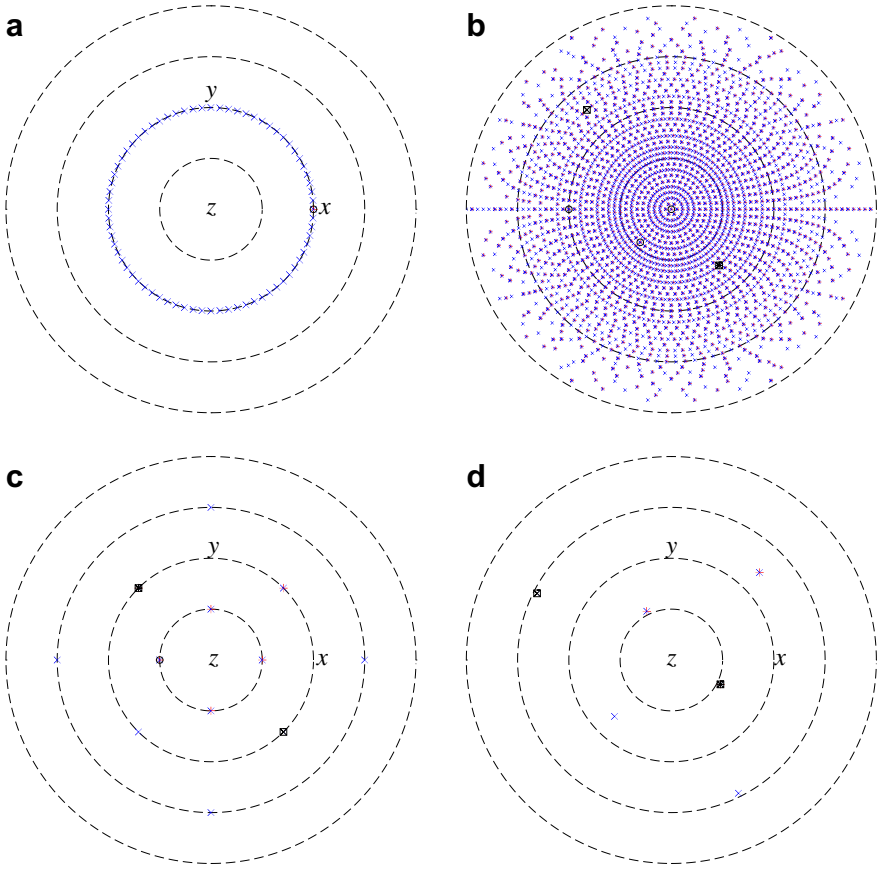

Fig. 1. Polar plots of the orientations used for the first (+) and second (×) wave vector in the different direction schemes where the longitude corresponds to the angle and the radius to the latitude (azimuth angle): (a) an example for a "circle" scheme with the first wave vector oriented along x and the second wave vector sampling a circle in the xy plane, (b) the "isotropic" scheme involving 1651 directions for the first wave vector uniformly distributed over the sphere, (c) the "tensor" scheme with six non-collinear directions for the first wave vector, respectively, and (d) one of the "trace" schemes used with three orthogonal directions for the first wave vector. In (b), (c), and (d), the directions of the second wave vector covered those of the first wave vector plus their counterparts with inverted polarity. The distance from the center is proportional to the azimuth angle with the dashed circles corresponding to $\pi/4$, $\pi/2$ (equator), i.e. the xy plane, $3\pi/4$, and π (south pole), i.e. $-z$ direction. The directions the plots of Figs. 3 and 4a are based on are marked with a circle in (b) and (c), respectively. Examples for directions with parallel and antiparallel orientations of the first and second wave vector are marked with a box in (b), (c), and (d).

equator (steps of 5°) yielding a total number of 1651 directions. For the second wave vector, these 1651 directions plus their 1651 counterparts with inverted polarities were used to ensure sampling of the parallel and antiparallel orientation for each of the directions of the first wave vector yielding 3302 directions in total.

The analysis of the according simulations involved the mentioned averaging of all signals obtained with the same θ enclosed by any of the first and any of the second wave vectors. Thereby, all combinations of the 1651 directions for the first with the 3302 directions of the second wave vector were analyzed with θ being rounded to multiples of 5° to ensure that the averaging was performed over a sufficiently large range of different wave vector orientations. A cosine-shaped angular dependency, independent of the pore geometry, should be observed for these analysis and $\langle R^2 \rangle$ can be estimated.

However, these simulations can also be used to confirm the presented tensor approach if the individual signal obtained for the different combinations of the first and second wave vector orientation are considered. For non-spherical pores they not only depend on θ but also on the orientation of the two wave vectors relative to the pores and are expected to obey Eq. (17). Thus, the full tensor $\underline{\underline{\mathbf{T}}}$ can be determined from these signals. It was calculated with a Levenberg–Marquardt algorithm that fits Eq. (17) to the 1651×3302 signals obtained for each combination of the first and second wave vector. Considering only the signal difference observed for parallel and antiparallel orientations of the two wave vectors along the 1651 directions, an analogous fit to Eq. (26) was performed to determine the tensor $\underline{\underline{\mathbf{R}}}$. In both cases, R_{eff} was calculated from the tensor's traces.

In order to demonstrate the applicability of the presented tensor approach which implies that the pore geometry information of the tensors $\underline{\underline{\mathbf{T}}}$ or $\underline{\underline{\mathbf{R}}}$ can be derived from a reduced number of wave vector orientations, simulations with a so-called "tensor" direction scheme (Fig. 1c) were performed. It involves six non-collinear directions for the first wave vector $((1,1,0)/\sqrt{2}$, $(1,-1,0)/\sqrt{2}$, $(1,0,1)/\sqrt{2}$, $(-1,0,1)/\sqrt{2}$, $(0,1,1)/\sqrt{2}$, $(0,-1,1)/\sqrt{2})$ representing directions often used in diffusion tensor imaging. For the second wave vector, these directions plus their inverted polarities were used yielding 12 orientations. A Levenberg–Marquardt algorithm was used to fit the 72 and 12 individual signals obtained when combining all or only the first direction of the first wave vector with the 12 directions of the second wave vector, respectively, to Eq. (17) and estimate the elements of $\underline{\underline{\mathbf{T}}}$ and the pore size parameter. Furthermore, an analogous fit of the signal differences of parallel and antiparallel wave vector orientations observed for the six directions to Eq. (26) was performed to calculate the elements of $\underline{\underline{\mathbf{R}}}$ according to Eq. (26), respectively, and estimate the pore size parameter R_{eff}.

If the double wave vector experiment aims to measure the average pore size, the determination of the trace of the tensor $\underline{\underline{\mathbf{R}}}$ is ex-

pected to be sufficient. This can be achieved by using only three orthogonal directions for the first wave vector and these three directions plus their counterparts with opposite polarity for the second wave vector, e.g. as shown in Fig. 1d. Different variants of this "trace" direction scheme were used in the simulations with the first wave vector either oriented along the coordinate axes ((1,0,0), (0,1,0), (0,0,1)), using orientations optimized to minimize gradient durations for an orthogonal direction scheme ((2,2,−1)/3, (2,−1,2)/3, (−1,2,2)/3, Fig. 1d), or determined randomly with the boundary condition of orthonormality ((0.2251,0.5831,0.7806), (0.7849,−0.5834,0.2095), (−0.5776,−0.5654,0.5889)). From the six signals obtained for each scheme, $\langle R^2 \rangle$ can be calculated. It should be independent of the direction scheme chosen as long as it obeys orthonormality if the tensor approach is valid.

4. Results

Spherical pores were considered first to confirm the validity and check the accuracy of the simulation algorithm and parameters and to yield reference results for a macroscopically isotropic sample. For the circle schemes the angular modulations are in good agreement with the cosine shape of Eq. (3) and show only a minor variation of the pore radius of below 3% (data not shown).

Simulation results obtained with the isotropic direction scheme are summarized in Fig. 2. The angular dependency of the signal averaged over all wave vector orientations for a given θ (Fig. 2a) shows the cosine modulation with θ described by Eq. (3). The pore radius estimated from this curve is about 93% of the nominal value. In Fig. 2b, the signals obtained for the parallel and antiparallel orientation of the two wave vectors and their difference are plotted for all 1651 individual orientations simulated. Some minor, unexpected modulations, in particular for the parallel orientation of the two wave vectors, are observed and most likely are due to rounding errors. Correspondingly, a slight deviation from the spherical symmetry of the pore is obtained when fitting the signal difference to Eq. (26) yielding 92.5%, 94.6%, and 92.6% of the nominal radius for the three coordinate axes. The off-diagonal elements were below 3% of the diagonal elements. Thus, despite of a minor underestimation and a slight systematic anisotropy, the simulations can be considered to be in good agreement with the theoretical results obtained by Mitra.

In Fig. 3, simulated MR signals obtained for spheroidal pores are shown. For the circle direction scheme (Fig. 1a) which can be considered to be the simplest approach to investigate the angular dependency of the signal experimentally, a variety of modulation shapes is observed (Fig. 3a). They depend on the chosen circle plane and the orientation of the first wave vector and can deviate considerably from the cosine shape of spherical pores or isotropic

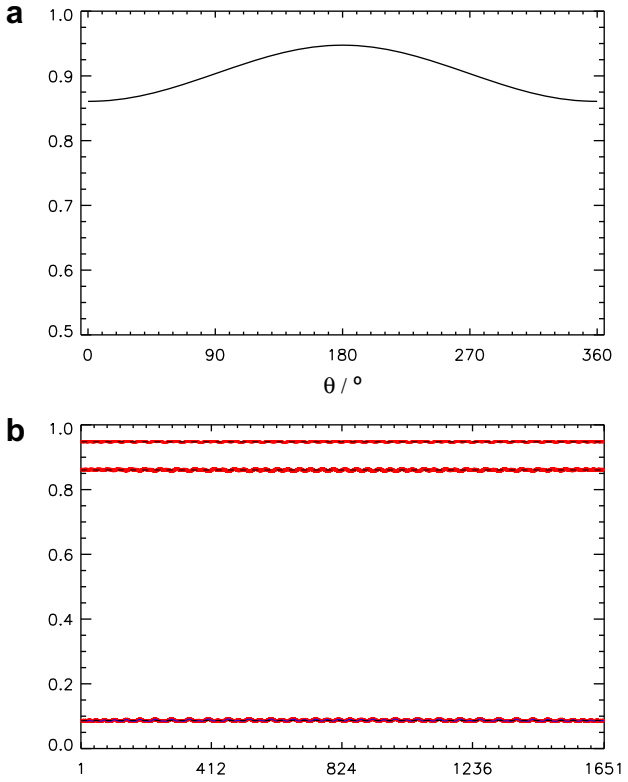

Fig. 2. Simulated MR signal of 10,000 particles diffusing in spherical pores observed in a double wave vector experiment using the isotropic direction scheme of Fig. 1b, (a) averaged over all combinations of the first and second wave vector that span an angle θ plotted vs. θ and (b) for parallel (middle) and antiparallel (upper) orientations of the two wave vectors and their difference (lower) for the 1651 different directions of the scheme (abscissa). The modulation curve of (a) well agrees with the cosine shape predicted by Mitra. (b) The dashed lines represent the average value of the corresponding simulated data, the solid line the fit of the signal difference to Eq. (26). The pore sizes derived from the fits yield about 93% of the nominal pore radius for both plots. For more details see text.

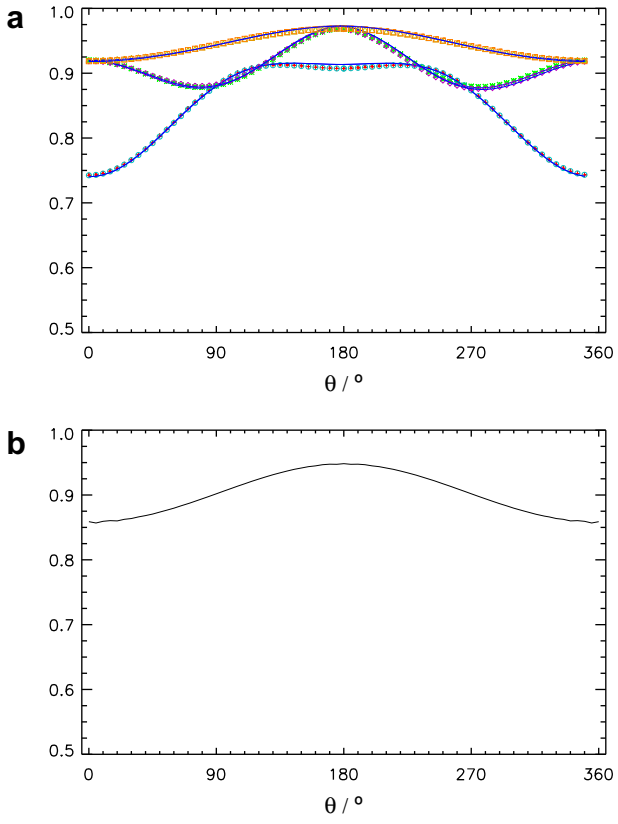

Fig. 3. Simulated MR signals obtained for 10,000 particles diffusing in prolate spheroidal pores (principal axis ratio 1.825, same effective pore radius as the spherical pore used for Fig. 2) with a single pore orientation. (a) Simulation results (symbols) obtained for the six different circle schemes (see Fig. 1a) where the first wave vector is fixed and the second samples a circle, plotted vs. the angle θ enclosed by the two wave vectors. Most of the modulations deviate from the cosine shape observed in samples with isotropic orientation distribution. The solid lines represent individual fits of Eq. (17) to the simulated data and yielded typical deviations of about ±3% from the nominal values. (b) The signal obtained for the isotropic direction scheme (see Fig. 1b) averaged over all combinations of the first and second wave vector that span an angle θ plotted vs. θ. A cosine-shaped curve is obtained which yields a pore size of about 96% of the nominal value. For more details see text.

orientation distributions which hampers a proper estimation of the pore size on the basis of such an experiment.

In contrast, the fits to Eq. (17) independently performed for each of the curves are in good agreement with the simulated data (Fig. 3a). Pore radii within the circle planes derived from these fits were typically within ±3% of the nominal values with peak deviations of −4% and +8%. For the chosen pore orientation, off-diagonal elements of $\underline{\underline{\mathbf{R}}}$ should vanish. For one curve, an off-diagonal element with a value of 5% of the minimum diagonal element was obtained but in all other cases the off-diagonal elements were below 1% of the diagonal elements. These results demonstrate the ability of the presented tensor approach to describe the signal behavior and to determine pore or cell geometry parameters for a simple double wave vector experiment in the more general case.

The signal obtained when averaging all contributions of the isotropic direction scheme with the same θ (Fig. 3b) shows the expected cosine modulation. It is very similar to the curve obtained for spherical pores (see Fig. 2a) and yields a mean pore diameter of about 96% of the nominal value. Thus, it is shown that the isotropic direction scheme (i) is able to reproduce the signal typical for an isotropic pore orientation distribution in a sample which has an anisotropic orientation distribution and (ii) yields a good estimate of $\langle R^2 \rangle$ in such samples.

Because the presented tensor approach is supposed to describe the signal behavior for any wave vector orientations relative to the orientation of the pore, the individual signal contributions obtained with the isotropic direction scheme were also analyzed in a different manner. The signals simulated for each of the 1651×3302, i.e. 5,451,602, wave vector combinations were fitted to Eq. (17) to determine $\underline{\underline{\mathbf{T}}}$. The pore radii derived from the tensor elements of $\underline{\underline{\mathbf{T}}}$ were in good agreement with the real value yielding about 97.6%, 99.5%, and 100.5% of the nominal values and all off-diagonal elements below 2% of the minimum diagonal element. Fig. 4 presents a fraction of the simulated data covering 1651 directions of the second wave vector for three different directions of the first one (Fig. 4a–c, respectively) together with the curve described by Eq. (17) using the tensor $\underline{\underline{\mathbf{T}}}$ determined from the fit. Considering that only six parameters, the independent tensor elements of $\underline{\underline{\mathbf{T}}}$, are used to approximate the more than 5.4 million data points a rather good agreement of the theoretical curve with the simulated data is observed which demonstrates the validity of the presented tensor formalism.

Having shown that the simulated data can be well described by the six independent tensor elements of $\underline{\underline{\mathbf{T}}}$, it is straightforward to investigate whether the number of wave vector directions, and thus the acquisition time in experiments, can be reduced without deteriorating the reliability or accuracy of the results. Simulations obtained with the tensor direction scheme are shown in Fig. 5 together with their fits (solid lines) to Eq. (17). Considering all 72 combinations of the orientations of the first (6 directions) and the second (12 directions) wave vector delivers the plot shown in Fig. 5a. The corresponding fit is in good agreement with the simulated data and yields radii of 98.0%, 99.1%, and 100.1% of the nominal values with off-diagonal elements of $\underline{\underline{\mathbf{T}}}$ which are below 2% of the minimum diagonal element. Thus, the deviations from the real values are as marginal as for the isotropic direction scheme although the number of data points has been reduced considerably.

To further reduce the number of directions, a subset of the simulations with the tensor direction scheme covering only one direction for the first wave vector, yielding twelve data points, was analyzed separately (Fig. 5b). The parameters of this fit correspond to radii of 98.6%, 103.2%, and 98.8% of the nominal values with all off-diagonal elements of $\underline{\underline{\mathbf{T}}}$ being below 3% of the minimum diagonal element which still is comparable to those obtained for the isotropic scheme. These results demonstrate that the tensor elements, and thus the pore geometry parameters and R_{eff}, can be reliably determined from a few wave vector directions, which in practice considerably reduces the acquisition time.

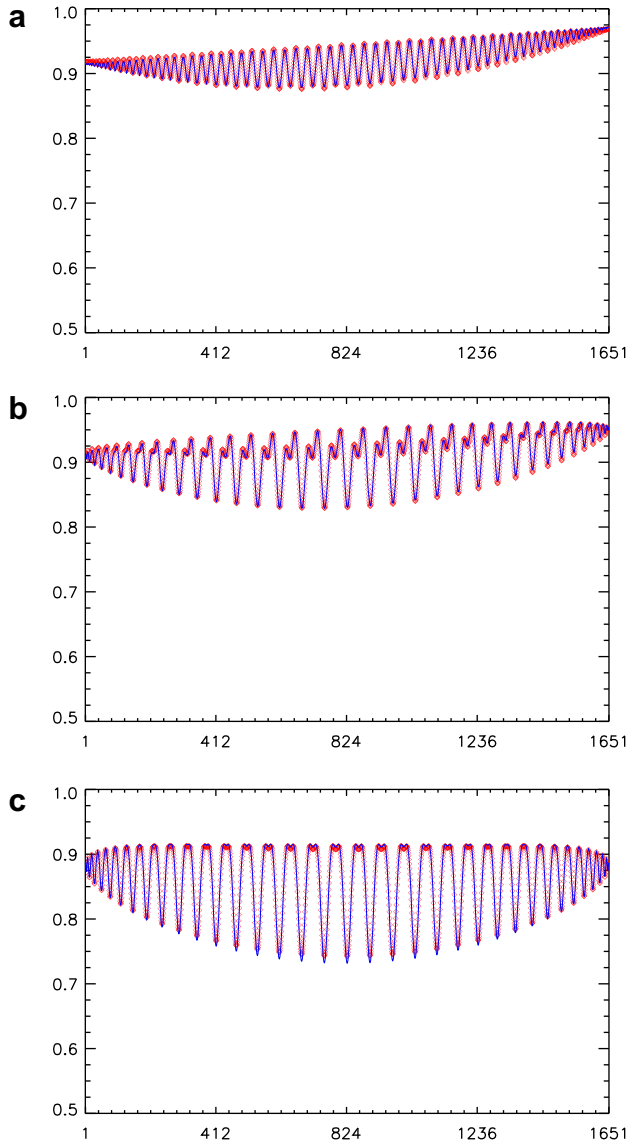

Fig. 4. Subset of the simulations of the MR signal performed with the isotropic direction scheme shown in Fig. 1b for the spheroidal pores. The simulated signal (diamonds) is shown for three different directions of the first wave vector (a–c, marked by the circles in Fig. 1b) and 1651 directions of the second wave vector (abscissa). The solid lines represent the fit of Eq. (17) to the full set of simulated signals covering more than 5.4 million data points, i.e. a single tensor $\underline{\underline{\mathbf{T}}}$ describes all fit curves shown in (a–c). The pore radii calculated from the fit deviated less then 3% from the nominal value. For more details see Fig. 3 and text.

As pointed out in Section 2, it is sufficient and expected to be advantageous to sample only parallel and antiparallel orientations of the two wave vectors. Fig. 6 summarizes the corresponding results obtained for the different direction schemes showing the individual signals for the parallel and the antiparallel orientations and their difference, respectively, for all orientations of the first wave vector. The modulation of the curves observed for the isotropic direction scheme (Fig. 6a) is due to the spheroidal pore shape which yields a more pronounced signal attenuation, and also an increased signal difference, for the longer principal axis. The fit to Eq. (26) is in good agreement with the simulations and yields 95%, 95%, and 96% of the nominal pore radii and off-diagonal elements of $\underline{\underline{\mathbf{R}}}$ below 1% of the diagonal elements. This can be considered

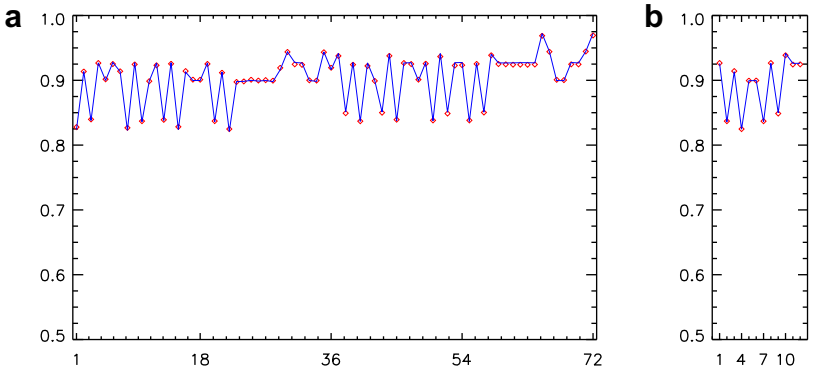

Fig. 5. Simulated MR signals (diamonds) obtained in the spheroidal pores for the tensor direction scheme (Fig. 1c) using (a) one (marked with the circle in Fig. 1c) and (b) all six directions for the first wave vector and twelve directions of the second wave vector. The solid lines represent individual fits of the simulations to Eq. (17) and yielded pore radii which were within ±3% of the nominal value. For more details see Fig. 3 and text.

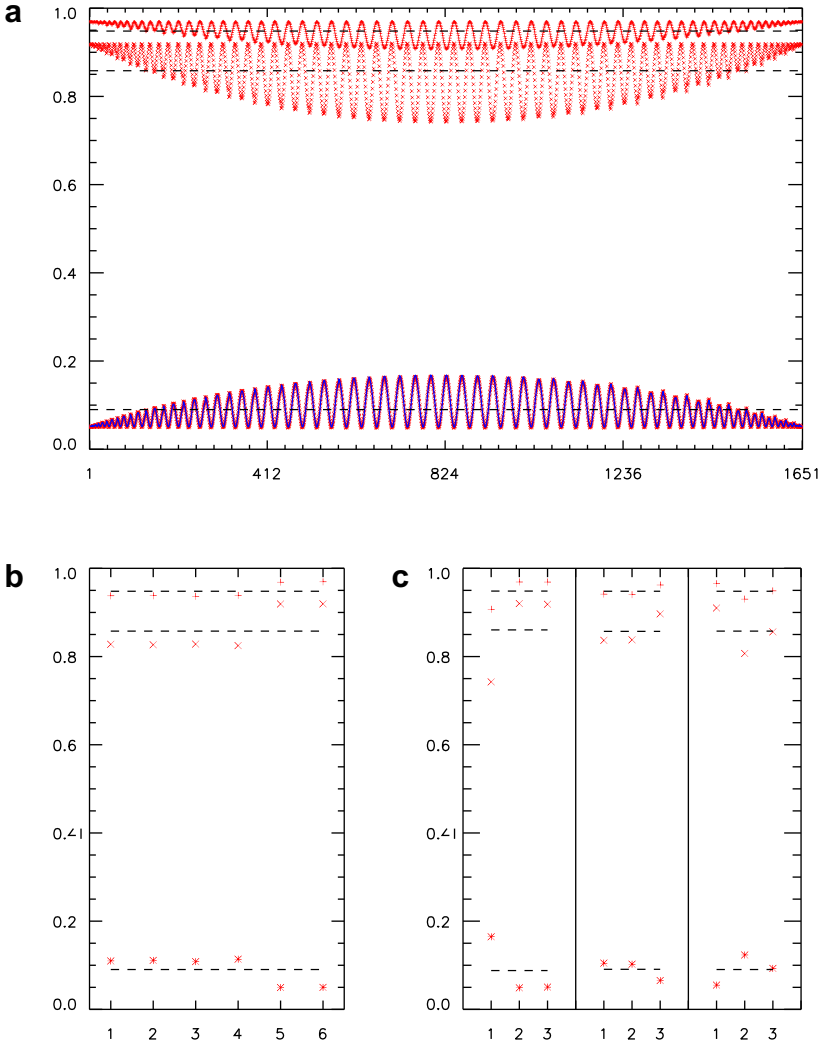

Fig. 6. Simulated MR signals (diamonds) in the spheroidal pores for parallel (×, middle) and antiparallel (+, top) orientation of the wave vectors and their difference (*, bottom) for different orientations of the first wave vector (abscissa) using the (a) isotropic direction scheme (1651 directions, Fig. 1b), (b) the tensor direction scheme (6 directions, Fig. 1c), and (c) the three different trace directions schemes (three directions each, example shown in Fig. 1b). Dashed horizontal lines represent the average over all directions and yield very similar results for all schemes with effective pore sizes varying only by about 2%. Furthermore, they are in good agreement with the results of Fig. 2b which was obtained with spherical pores with the same effective pore size. The solid line in (a) represents the fit of the signal difference to Eq. (26). For more details see Fig. 3 and text.

to be less accurate than analyzing the full angular coverage but is expected to be a consequence of the additional modulations which have been observed for the parallel wave vector orientation, e.g. in Fig. 2b for the spherical pores, and which most likely represent a numerical but not a physical effect. The averages of the signals (0.9483 and 0.8589) and their difference (0.0895) are very similar

to those obtained for the spherical pores (0.9475, 0.8606, and 0.08687, respectively; compare Fig. 2b) and reflect the identical $\langle R^2 \rangle$ of both pore geometries. The corresponding results for the tensor direction scheme are shown in Fig. 6b. A signal difference of 0.0904 is observed which delivers, to an accuracy of about 1%, the same R_{eff} as the isotropic scheme. Thus, Eq. (26) seems to provide a reasonable description for the signal difference of parallel and antiparallel wave vector orientations.

The results for the trace direction schemes are shown in Fig. 6c. From their data not the full tensor information but only the trace of $\underline{\underline{\mathbf{R}}}$ can be determined which however is sufficient to estimate R_{eff}. The individual signals and the difference of parallel and antiparallel orientations show a large variability depending on the specific orientations used and almost cover the full range of signal amplitudes and differences observed for the isotropic scheme. However, the signal difference averaged over the three orthogonal directions of each scheme yields values of 0.0880, 0.0909, and 0.0904, being quite constant and resulting in an R_{eff} value deviation within 2% of that obtained for the isotropic mode. Thus, a rotationally invariant pore or cell size measure can be obtained accurately from a simple measurement involving only six acquisitions in addition to one without diffusion weighting which considerably simplifies double wave vector experiments that aim to determine pore or cell sizes in samples with an unknown or non-isotropic pore or cell orientation distribution.

5. Discussion

The theoretical derivations of Mitra have been re-investigated in order to derive a more general expression for the signal in double wave vector diffusion-weighting experiments of restricted diffusion that does not assume an isotropic orientation distribution of the pores or cells within the sample. Two rank-2 tensors with six independent elements can be used to describe the signal in terms of the wave vectors, either for an arbitrary combination of wave vectors ($\underline{\underline{\mathbf{T}}}$, 6×6, six independent elements) or for the signal difference of parallel and antiparallel wave vector orientations ($\underline{\underline{\mathbf{R}}}$, 3×3, six independent elements). Thus, only a small number of diffusion-weighting measurements is required to obtain a description of the signal behavior for the general experiment. Furthermore, a rotationally invariant measure of the pore size can be derived from the traces of $\underline{\underline{\mathbf{T}}}$ and $\underline{\underline{\mathbf{R}}}$ which can be determined using three orthogonal orientations only. This further shortens the acquisition times in experiments targeting the pore or cell size.

The numerical simulations of the MR signal for diffusion in spherical and prolate spheroidal pores are in good agreement with the theoretical expectations. The theoretical results of Mitra for an isotropic orientation distribution were confirmed. In the more general case, the complex angular signal dependency can be well approximated with the equations derived, using the six independent elements of the tensors $\underline{\underline{\mathbf{T}}}$ and $\underline{\underline{\mathbf{R}}}$ as degrees of freedom. The pore sizes estimated from a fit of the model to the simulated data are in good agreement with the nominal values with typical deviations of about or below 5% which demonstrates the validity of the presented theoretical approach.

There seems to be a slight but systematic underestimation of the pore size when applying the tensor model to the numerical simulations performed, e.g. for the spherical pores. Most likely this is due to higher (4th) order contributions in the simulated signal which were not taken into account in the theory. These contributions may also explain the more pronounced size deviations for the analysis considering only parallel and antiparallel gradient orientations where the acquisitions with a higher diffusion-induced signal decay have a higher relative weighting.

Some systematic angular modulation was observed for the simulations of spherical pores, in particular for the parallel orientation of the two wave vectors, which also yields a slightly non-spherical pore shape even for spherical pores. It is conjectured that these modulations are due to rounding errors that may not exactly yield (i) wave vectors with identical length for the different orientations and (ii) a perfectly spherical pore shape. It also may be possible that the hidden algorithm of the random number generator also has some influence on these artifacts. Nevertheless, the observed modulations are well below those observed for the spheroidal pores and are not expected to have a significant influence on the results.

An extension of the presented tensor approach could take finite gradient pulse lengths δ, diffusion time Δ, and mixing time τ_{m} into account, e.g. by using the expressions derived recently by Özarslan et al. [14]. This would allow a better approximation of real experiments where the assumptions underlying the presented model ($\delta \to 0$, $\Delta \gg \tau_{\mathrm{D}}$) usually are not fulfilled. However, these calculations are expected to be rather challenging and may only yield solutions if a specific pore geometry is assumed which would be of limited value for biological tissue where exact information about the microscopic tissue geometry may be difficult to obtain.

6. Conclusions

A tensor approach to double wave vector diffusion-weighting experiments on restricted diffusion has been presented which allows to model the signal behavior in the general case of an arbitrary orientation distribution of the pores or cells. Six independent tensor elements, which could be determined from as few as six diffusion-weighted measurements, are sufficient to describe the experiment for arbitrary wave vectors, three of which can be used to determine the trace of the tensor which allows to estimate a rotationally invariant measure for the pore or cell size. Thus, the presented approach may help to improve the applicability of double wave vector experiments for pore or cell size estimation, in particular in biological tissue.

Acknowledgments

Parts of this work were supported by Deutsche Forschungsgemeinschaft and Bundesministerium für Bildung und Forschung (Neuroimage Nord).

Appendix A

First, an isotropic orientation distribution of the identical pores is assumed yielding

$$\underline{\underline{\mathbf{R}_{\mathbf{iso}}}} = \frac{1}{4\pi} \int_{4\pi} \underline{\underline{\mathbf{R}}} \, \mathrm{d}\Omega \tag{A.1}$$

which for $\rho(\mathbf{r}) = \rho$ is given by

$$(R_{\mathrm{iso}})_{ij} = \frac{1}{4\pi} \rho \int_{4\pi} \int_{\mathrm{pore}} r_i r_j \, \mathrm{d}\mathbf{r} \, \mathrm{d}\Omega = \frac{1}{3} \rho \int_{\mathrm{pore}} r_i r_j \delta_{ij} \, \mathrm{d}\mathbf{r}. \tag{A.2}$$

M then is given by

$$M_{\mathrm{iso}}(\mathbf{Q}) \propto V - \frac{1}{2} \mathbf{Q}^{\mathrm{T}} \begin{pmatrix} 2\underline{\underline{\mathbf{R}_{\mathrm{iso}}}} & \underline{\underline{\mathbf{R}_{\mathrm{iso}}}} \\ \underline{\underline{\mathbf{R}_{\mathrm{iso}}}} & 2\underline{\underline{\mathbf{R}_{\mathrm{iso}}}} \end{pmatrix} \mathbf{Q} \tag{A.3}$$

which delivers

$$\begin{aligned} M_{\mathrm{iso}}(\mathbf{Q}) &\propto V - \frac{1}{6} \rho \int_{\mathrm{pore}} r^2 \, \mathrm{d}\mathbf{r} \mathbf{Q}^{\mathrm{T}} \begin{pmatrix} 2\underline{\underline{\mathbf{1}}} & \underline{\underline{\mathbf{1}}} \\ \underline{\underline{\mathbf{1}}} & 2\underline{\underline{\mathbf{1}}} \end{pmatrix} \mathbf{Q} \\ &= V - \frac{1}{6} \rho \int_{\mathrm{pore}} r^2 \, \mathrm{d}\mathbf{r} \left(2Q^2 + \mathbf{Q}^{\mathrm{T}} \begin{pmatrix} 0 & \underline{\underline{\mathbf{1}}} \\ \underline{\underline{\mathbf{1}}} & 0 \end{pmatrix} \mathbf{Q} \right) \end{aligned} \tag{A.4}$$

or when re-substituting $\mathbf{Q}$ by $\mathbf{q_1}$ and $\mathbf{q_2}$

$$M_{\mathrm{iso}}(\mathbf{q_1},\mathbf{q_2}) \propto V - \frac{1}{6}\rho \int_{\mathrm{pore}} r^2\,\mathrm{d}\mathbf{r}(2q_1^2 + 2q_2^2 + 2\mathbf{q_1}\mathbf{q_2}). \tag{A.5}$$

For $|\mathbf{q_1}| = |\mathbf{q_2}| = q$, using θ for the angle between $\mathbf{q_1}$ and $\mathbf{q}_2$, i.e. $\cos\theta = \mathbf{q_1}\mathbf{q_2}/q^2$, and defining

$$\langle R^2\rangle = \int_{\mathrm{pore}} r^2\,\mathrm{d}\mathbf{r} \tag{A.6}$$

Eq. (A.5) simplifies to

$$M_{\mathrm{iso}}(\mathbf{q_1},\mathbf{q_2}) \propto V - \frac{1}{3}\rho q^2\langle R^2\rangle(2+\cos\theta) \tag{A.7}$$

which corresponds to the result reported by Mitra.

It should be noted that the result holds for a mixture of pore populations as long as each population has an isotropic orientation distribution. $\langle R^2\rangle$ then has to be replaced by the averaged sum of the individual $\langle R^2\rangle_j$.

Appendix B. Supplementary data

Supplementary data associated with this article can be found, in the online version, at doi:10.1016/j.jmr.2008.08.003.

References

[1] E.O. Stejskal, J.E. Tanner, Spin diffusion measurements: spin echoes in the presence of a time-dependent field gradient, J. Chem. Phys. 42 (1965) 288–292.
[2] D.G. Cory, A.N. Garroway, J.B. Miller, Applications of spin transport as a probe of local geometry, Polym. Preprints 31 (1990) 149–150.
[3] P.T. Callaghan, B. Manz, Velocity exchange spectroscopy, J. Magn. Reson. A 106 (1994) 260–265.
[4] P.T. Callaghan, D. MacGowan, K.J. Packer, F.O. Zelayam, High-resolution q-space imaging in porous structures, J. Magn. Reson. 90 (1990) 177–182.
[5] P.P. Mitra, Multiple wave-vector extensions of the NMR pulsed-field-gradient spin-echo diffusion measurement, Phys. Rev. B 51 (1995) 15074–15078.
[6] Y. Cheng, D.G. Cory, Multiple scattering by NMR, J. Am. Chem. Soc. 121 (1999) 7935–7936.
[7] M.E. Komlosh, F. Horkay, R.Z. Freidlin, Y. Assaf, P.J. Basser, Detection of microscopic anisotropy in gray matter using d-PGSE, in: Proceedings of 13th Annual Meeting on the International Society for Magnetic Resonance in Medicine, Miami Beach, USA, 2005, p. 843.
[8] M.E. Komlosh, F. Horkay, R.Z. Freidlin, U. Nevo, Y. Assaf, P.J. Basser, Detection of microscopic anisotropy in gray matter and in a novel tissue phantom using double pulsed gradient spin echo MR, J. Magn. Reson. 189 (2007) 38–45.
[9] M.E. Komlosh, M.J. Lizak, F. Horkay, R.Z. Freidlin, P.J. Basser, Observation of microscopic diffusion anisotropy in the spinal cord using double-pulsed gradient spin echo MRI, Magn. Reson. Med. 59 (2008) 803–809.
[10] P.T. Callaghan, I. Furó, Diffusion–diffusion correlation and exchange as a signature for local order and dynamics, J. Chem. Phys. 120 (2004) 4032–4038.
[11] M.A. Koch, J. Finsterbusch, Multiple wave vector diffusion experiments on restricted diffusion, in: Proceedings of 13th Annual Meeting on the International Society for Magnetic Resonance in Medicine, Miami Beach, Germany, 2005, p. 840.
[12] M.A. Koch, J. Finsterbusch, Compartment size estimation with double wave vector diffusion-weighted imaging, Magn. Reson. Med. 60 (2008) 90–101.
[13] C.H. Ziener, T. Weber, W.R. Bauer, P.M. Jakob, Quantification of the spinal cord axon diameter using an extension of the PGSE sequence, in: Proceedings of 15th Annual Meeting on the International Society for Magnetic Resonance in Medicine, Berlin, Germany, 2007, p. 13.
[14] E. Özarslan, P.J. Basser, Microscopic anisotropy revealed by NMR double pulsed field gradient experiments with arbitrary timing parameters, J. Chem. Phys. 128 (2008). 154511-1–154511-11.